A modified W–W interatomic potential based on *ab initio* calculations

A modified W–W interatomic potential based on *ab initio* calculations

J Wang, Y L Zhou, M Li and Q Hou

Key Laboratory for Radiation Physics and Technology, Institute of Nuclear Science and Technology, Sichuan University, Chengdu 610064, People's Republic of China

E-mail: qhouscu@163.com

Abstract

In this paper we have developed a Finnis–Sinclair-type interatomic potential for W–W interactions that is based on *ab initio* calculations. The modified potential is able to reproduce the correct formation energies of self-interstitial atom (SIA) defects in tungsten, offering a significant improvement over the Ackland–Thetford tungsten potential. Using the modified potential, the thermal expansion is calculated in a temperature range from 0 to 3500 K. The results are in reasonable agreement with the experimental data, thus overcoming the shortcomings of the negative thermal expansion using the Derlet–Nguyen–Manh–Dudarev tungsten potential. The W–W potential presented here is also applied to study in detail the diffusion of SIAs in tungsten. We reveal that the initial SIA initiates a sequence of tungsten atom displacements and replacements in the $\langle 1\,1\,1 \rangle$ direction. An Arrhenius fit to the diffusion data at temperatures below 550 K indicates a migration energy of 0.022 eV, which is in reasonable agreement with the experimental data.

Keywords: tungsten potential, vacancy, self-interstitial atom, molecular dynamics simulations

1. Introduction

Due to its high melting point, high thermal conductivity, and low sputtering erosion, tungsten is a promising candidate for plasma facing materials in fusion applications (e.g. for the divertor armor of future thermonuclear fusion reactors) [1, 2]. However, in this application the tungsten will be subjected to high-energy neutron irradiation, which produces vacancies and self-interstitial atoms (SIAs) due to atomic displacements. It also generates helium by transmutation reactions throughout its lifetime. The accumulation and interaction of these defects in plasma facing materials is believed to produce swelling, cause embrittlement and induce blisters, ultimately resulting in the deterioration of the mechanical properties of the

material. Understanding and predicting these important physical processes has been a subject of considerable interest [3–10].

　　Molecular dynamics (MD) simulations, as one of the most effective and powerful tools in materials science, are extensively used to study many physical processes (such as defect formation and its influence on the mechanical properties of materials). An appropriate description of the interatomic potentials is of critical importance for the reliable performance of MD simulations. Hence, significant effort has been dedicated to developing accurate W–W potentials, such as the Finnis–Sinclair (FS) potential [11], the embedded atom method (EAM) [12], the modified embedded atom method (MEAM) [13], the bond-order potential with Tersoff–Brenner-type form (BOP) [14, 15], and the bond-order potential based on the tight-binding approximation (TB-BOP) [16]. Among these potentials, the FS-type potential is very attractive because of its simple analytic formalism and high computational efficiency. The most commonly used potential is the Ackland–Thetford (AT) potential [17], which was developed from the FS potential [11] and which is able to predict a realistic pressure–volume relationship; however, compared to the *ab initio* calculations, the obtained SIA formation energies are entirely too low and the energy differences between various SIA configurations are quite different from those of the *ab initio* calculations [9, 10]. Recently, Derlet *et al* developed a FS-type potential (hereafter DND) that is fitted to the *ab initio* calculations and which is able to reproduce the correct energies of various SIA configurations in tungsten [18]; however, it predicts negative thermal expansion when the temperature is above approximately 300 K, which is in conflict with the experimental results [5, 19, 20].

　　The MD simulations performed by Fikar *et al* demonstrated that different W–W potentials result in different defect behavior [4, 5]. Our previous study also indicated that different W–W potentials have a significant influence on the He defect properties in tungsten [21]. Due to the shortcomings of the AT and DND potentials mentioned above, a more reliable W–W potential is necessary to investigate the defect behavior in tungsten in a more accurate way. In this paper, we propose an FS-type interatomic potential for W–W interactions on the basis of *ab initio* calculations to investigate the defect properties and SIA diffusion behavior in tungsten.

2. W–W interaction potential

According to the FS formalism [11], the total energy of an N-atom system is given by

$$E_{\text{tot}} = \sum_i^N F(\rho_i) + \frac{1}{2} \sum_{ij, i \neq j}^N V(r_{ij}), \tag{1}$$

where the embedding energy $F(\rho)$ is given by

$$F(\rho) = -A\sqrt{\rho}, \tag{2}$$

and

$$\rho_i = \sum_{j, j \neq i} f(r_{ij}). \tag{3}$$

For this work, the pairwise potential function and the electronic density function will be represented by a series of polynomial functions,

$$f(r) = \sum_{n=1}^N (A_n + B_n r + C_n r^2 + D_n r^3 + E_n r^4 + F_n r^5 + G_n r^6 + H_n r^7) \Theta(r_n - r) \Theta(r - r_{n+1}),$$
$$r_1 < r \leqslant r_{N+1} \tag{4}$$

and

$$V(r) = \sum_{n=1}^{N'} (A'_n + B'_n r + C'_n r^2 + D'_n r^3 + E'_n r^4 + F'_n r^5 + G'_n r^6 + H'_n r^7)\Theta(r'_n - r)\Theta(r - r'_{n+1}),$$
$$r'_1 < r \leqslant r'_{N+1}, \tag{5}$$

respectively, where $\Theta(x)$ is a Heaviside step function, defined as $\Theta(x) = 1$ for $x \geqslant 0$ and $\Theta(x) = 0$ for $x < 0$.

To obtain a usable empirical potential, the potential parameters from these functions given above are optimized using a genetic algorithm [22], which is combined with MD simulations to reproduce as closely as possible a variety of physical properties for tungsten. At the intersection points, the function values and their first derivatives are guaranteed to be continuous. In this study, in addition to the basic physical properties (i.e. lattice constant, cohesive energy, elastic constants and vacancy formation), the SIA defect formation energies from the *ab initio* calculations [10] are also included, as listed in table 1. Considering computer capacity, all simulations were performed for 432 atoms in pure bulk, adding or removing atoms as needed for the defect configuration. Periodic boundary conditions and constant volume were used for all simulations. Because the process for determining the optimal parameters is a rather complex process, a manual interruption is often required to produce the desired properties. While a set of optimal parameters are obtained, the basic properties (such as SIA formation energies) and other properties (such as thermal expansion) that are not included in the fitting are examined for the purpose of obtaining a more reliable potential. The resulting parameters are presented in table 2. For reference, figure 1 displays the electronic density function multiplied by A^2 and pairwise potential radial function for AT, DND and the tungsten potentials presented here. As seen in table 1, the basic physical properties and SIA defect properties are reproduced well. The $\langle 1\,1\,1 \rangle$ dumbbell is determined to be the most stable configuration in tungsten, its formation energy is 9.58 eV, and the difference with the $\langle 1\,1\,0 \rangle$ dumbbell is 0.28 eV, which is in excellent agreement with the *ab initio* calculations [9, 10]. The potential presented here offers a significant improvement over the W–W potential of Ackland *et al* [17]. In the following section, we will see that it also improves the DND potential by investigating the thermal expansion.

3. Structural stability

In the fitting procedure, we do not consider the properties of other crystal structures, such as the equilibrium lattice constant for face-centered cubic (fcc) structure. However, it is known that the stability of the ground-state bcc structure relative to other crystal structures is very important when testing the reliability of a potential. Based on the newly constructed potential, the cohesive energies and lattice constants have been calculated for several high-symmetry structures, namely: A15, fcc, simple cubic (sc), and diamond structures. The related data from the AT potential, the DND potential, the BOP potential [15], and the TB-BOP [16] potential are also presented. From table 3, one can clearly see that the bcc structure is the most stable. Even though the lattice constants of the A15 structure are nicely reproduced, the cohesive energy of A15 is less satisfactory when compared with *ab initio* results, which is similar to most of the existing potentials.

4. Thermal expansion and melting point

Thermal expansion is a critical characteristic property of all materials. Here, the linear thermal expansion is employed, whose form is expressed as follows:

$$\beta(T) = [L(T) - L_0]/L_0, \tag{6}$$

Table 1. Comparison of the properties of bcc tungsten as obtained from experiment, *ab initio* calculations, the AT potential, the DND potential, and the modified FS potential derived in the this study. E_c: cohesive energy (eV/atom); a: lattice parameter (nm); B: bulk modulus (GPa); C_{ij}: elastic constants (GPa); T_m: melting point; E_{vac}^f and E_{vac}^m are the vacancy formation energy (eV) and the vacancy migration energy (eV), respectively; E_{d111}^f, E_{d110}^f, E_{d100}^f are the formation energies (eV) of SIAs with $\langle 1\,1\,1 \rangle$, $\langle 1\,1\,0 \rangle$ and $\langle 1\,0\,0 \rangle$ configurations, respectively; E_{tet}^f and E_{oct}^f are the formation energies (eV) of a SIA in tungsten for the tetrahedral and octahedral sites, respectively.

	This study	*Ab initio*	Experiment	DND[a]	AT[b]
E_c	−8.9	−9.97[c], −8.49[d]	−8.9[e]	−8.9	−8.9
a	0.3165	0.314[c], 0.3172[d]	0.3165[f]	0.3165	0.3165
B	309	320[g]	308–314[h]	310	310
C_{11}	520	552[g]	501–521[h]	525	522
C_{12}	204	204[g]	199–207[h]	203	204
C_{44}	161	149[g]	151–160[h]	159	161
E_{vac}^f	3.58	3.56[i], 3.11[j]	3.1–4.0[k,l]	3.56	3.63
E_{vac}^m	1.43	1.78[i],1.66[j]	1.7–2.0[m,n] 1.5 at 0 K[j,o]	2.07[p]	1.44[p]
E_{d111}^f	9.58	9.55[i], 9.82[j]		9.55	8.92
E_{d110}^f	9.86	9.84[i], 10.10[j]		9.84	9.64
E_{d100}^f	11.53	11.49[i], 11.74[j]		11.51	9.82
E_{tet}^f	10.93	11.05[i], 11.64[j]		11.00	10.00[p]
E_{oct}^f	11.72	11.68[i], 11.99[j]		11.71	10.02[p]
T_m	4100 ± 50		3695	3750[q]	5150–5250[q]

[a] Reference [18].
[b] Reference [17].
[c] Reference [27].
[d] Reference [15].
[e] Reference [28].
[f] Reference [29].
[g] Reference [30].
[h] Reference [31].
[i] Reference [10].
[j] Reference [8].
[k] Reference [32].
[l] Reference [33].
[m] Reference [34].
[n] Reference [35].
[o] Reference [26].
[p] This work.
[q] Reference [5].

where l_0 and l refer to the specimen length at reference temperature and at the temperature T, respectively. For comparison purposes, we set the reference temperature to 293.15 K, which is the same as that in the experiment [19]. The thermal expansions of three potentials (AT, DND and the potential presented here) were determined by relaxing the tungsten sample containing 2000 tungsten atoms at different temperatures using MD simulations. The temperature of the system was varied between 0 and 3500 K using an electron–phonon coupling model, in which the electron gas is considered as a thermostat at constant temperature. For each temperature, the system volume was adjusted to maintain a pressure of approximately 0 kbar. As shown in figure 2, the thermal expansion from the AT potential is significantly higher than that of

Table 2. Parameters for the W–W potential presented here. The units are combinations of eV and Å to have equations (1) to (5) expressed in units of eV.

A_n	B_n	C_n	D_n	
836.733 119 131 673	−1092.737 231 462 09	570.244 952 195 581	−149.176 023 687 989	
185.476 611 562 764	−65.153 190 570 516 0	−144.143 194 717 123	128.381 692 972 279	
4483.329 429 084 44	798.771 513 881 627	−3119.648 565 771 41	−2188.341 994 793 66	
497.885 673 416 326	−663.034 572 443 750	332.677 312 093 750	−74.418 864 850 000 0	
1033.670 919 880 25	−1124.853 812 867 82	408.726 035 584 526	−49.569 685 012 102 1	
10 782.439 943 326 6	−13 005.029 891 801 5	5 234.586 043 380 40	−703.009 068 965 912	

Potential parameters

E_n	F_n	G_n	H_n	r_n
19.759 095 653 944 9	−1.109 291 544 382 37	8.583 068 847 656 250E−3	0.0	4.252 700 349 688 53
−42.261 409 151 440 5	6.189 679 402 835 76	−0.329 017 639 160 156	0.0	3.187 984 227 538 11
3 852.657 076 057 29	−1773.506 980 787 52	352.122 068 405 151	−26.299 715 042 114 3	3.082 884 786 129 00
6.254 199 900 000 00	0.0	0.0	0.0	2.830 759 763 717 65
0.0	0.0	0.0	0.0	2.729 170 799 404 38
0.0	0.0	0.0	0.0	2.461 773 872 375 49

Potential parameters

A'_n	B'_n	C'_n	D'_n	
0.176 113 968 245 774	−4.427 276 514 331 02	6.085 963 670 851 00	−3.316 271 856 191 30	
−9.010 972 573 915 17	17.765 243 001 767 2	−14.044 818 238 256 2	5.852 629 817 503 76	
2941.476 635 263 72	−4976.299 952 140 59	3363.925 662 984 62	−1135.685 055 746 01	
−506.899 715 533 763	1117.191 383 468 61	−1025.008 653 140 71	501.406 917 325 721	
170.584 208 417 048	−191.839 109 698 533	72.002 548 363 439 9	−9.013 654 940 029 94	
98.579 868 220 765 4	−105.456 860 917 279	37.458 830 192 351 8	−4.409 049 704 119 85	

Potential parameters

E'_n	F'_n	G'_n	H'_n	r'_n
0.889 234 910 474 537	−0.117 663 809 722 679	6.163 730 456 134 172E−3	0.0	4.449 993 165 731 43
−1.368 491 208 875 94	0.170 647 289 763 123	−8.865 704 319 423 323E−3	0.0	3.269 859 552 383 42
191.481 369 497 020	−12.898 515 630 795 8	0.0	0.0	3.146 148 443 818 09
−137.946 827 388 616	20.238 676 690 490 3	−1.237 062 256 521 03	0.0	2.791 941 642 761 23
0.0	0.0	0.0	0.0	2.661 482 813 358 31
0.0	0.0	0.0	0.0	2.500 664 472 579 96

Potential parameters

N	N'	r_{N+1}	r'_{N+1}	A
6	6	0.0	0.0	10.363 276 064 395 9

the experimental results while for the DND a negative thermal expansion appears, which is in conflict with the experimental results [19, 20]. The thermal expansion is directly related to the interatomic potential of a crystal and is closely related to other thermodynamic and mechanical properties. In particular, high-temperature thermal expansion is most sensitive to the formation of thermal defects [20]. The potential presented here is able to correctly predict the thermal expansion, demonstrating that it is a reliable potential over a fairly broad temperature range.

Furthermore, the melting point was determined using the potential presented here by performing the MD simulations of a two phase system [14, 23, 24] with a 20 × 10 × 10 simulation box containing 4000 tungsten atoms. Solid and liquid phases were joined and relaxed to different temperatures. If the temperature is above the melting temperature, the interface moves into the solid region and the sample will melt completely with further evolution; otherwise, crystallization occurs. Here, the melting temperature is 4100±50 K, which is 400 K higher than the experimental value of 3695 K. According to the calculations performed by
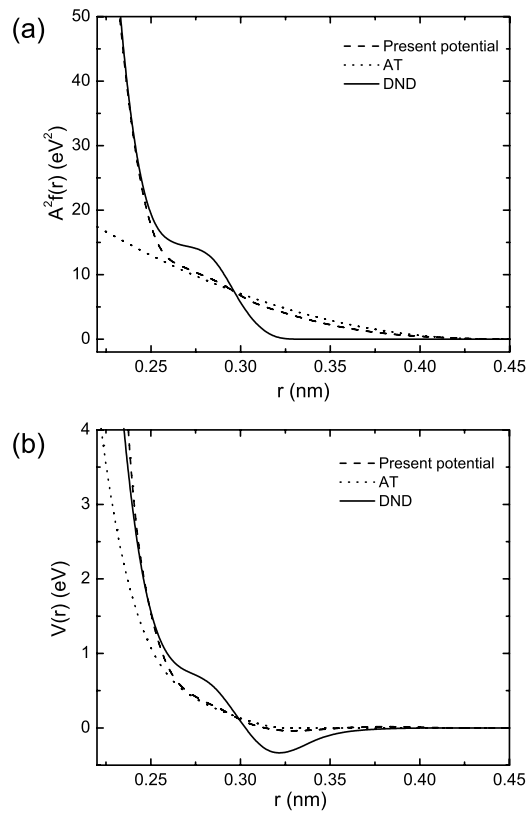
Figure 1. The present tungsten potential compared to the AT and DND potentials: (*a*) the electronic density function multiplied by A^2, and (*b*) the pairwise potential radial functions.

Fikar *et al*, the melting points determined using the AT and DND potentials are approximately 5200 K and 3750 K, respectively [5]. The melting point using the extended FS potential by Dai *et al* is 4500 K [25]. The melting points from the BOPs constructed by Juslin *et al* [14] and by Li *et al* [24] are 2750 K and 4500 K, respectively. The melting point using the MEAM potential is 4600 K [13]. Compared to most of the existing potentials, the potential presented here is able to reasonably reproduce the tungsten melting point. Note that, although the DND potential cannot correctly predict the thermal expansion, it can closely predict the melting point.

5. Point defect properties

With the present potential, the vacancy migration energy that is not included in the fitting was calculated using the drag method. The resulting vacancy migration energy is 1.43 eV. Although this is very close to the value obtained using the AT potential (1.44 eV), it is lower than the experimental value of 1.7–2.02 eV. However, as indicated by Becquart and Domain [8], the comparison to experimental results is not straightforward because the calculations were performed at 0 K while the experimental data were obtained at high temperatures. Thus, the vacancy migration energy should be compared with the experimental values extrapolated to 0 K; that is, 1.50 eV according to Satta *et al* [26]. From this viewpoint, the vacancy migration energy is reasonable.

Table 3. Comparison of the properties of several high-symmetry bulk phases of tungsten as obtained from experiment, DFT calculations, the AT potential, the DND potential, the BOP potential, the TB-BOP potential, and the modified FS potential derived in the this study. ΔE is the energy difference of the A15, fcc, sc and diamond structures with respect to a bcc one (eV/atom); a is the lattice constant (Å).

	Experiment	DFT	This study	DND[a]	AT[a]	TB-BOP[b]	BOP[c]
Diamond							
ΔE		2.33[d]	3.27	2.82	3.38		4.46
a		5.87[d]	6.19	6.34	6.08		6.01
sc							
ΔE		1.35[b]	1.75	1.81	1.37	1.23	2.07
a		2.61[b]	2.67	2.76	2.60	2.52	2.59
fcc, $\gamma - W$							
ΔE	0.2[d]	0.47[b], 0.49[c]	0.09	0.06	0.15	0.48	0.24
a		4.00[b], 4.02[c]	3.98	4.00	3.92	4.02	4.05
A15, $\beta - W$							
ΔE		0.08[b],0.09[c]	0.30	0.34	0.21	0.64	0.10
a	5.05[e]	5.06[b],5.06[c]	5.11	5.05	5.14	5.07	5.16

[a] This work.
[b] Reference [16].
[c] Reference [15].
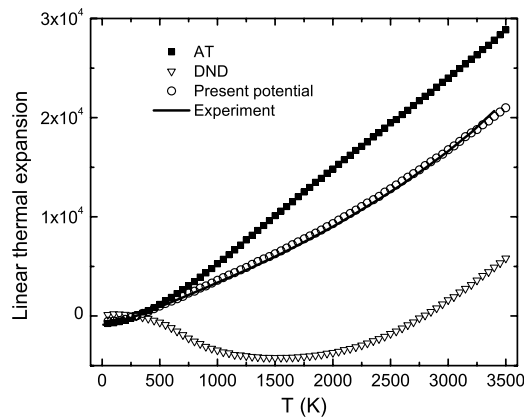[d] Reference [14].
[e] Reference [36].

Figure 2. Thermal expansion derived from the AT, DND and the potential presented here in comparison with the experimental results.

The properties of SIAs are of particular interest because their production, accumulation, and migration will greatly affect the mechanical properties of materials. In this work, the diffusion behavior of SIAs was investigated using MD simulations. The observed migration of a $\langle 1\,1\,1 \rangle$ SIA, which is the most stable SIA configuration, is one-dimensional in the $\langle 1\,1\,1 \rangle$ direction at temperatures below 550 K. For the convenience of analyses, the atom that is located closest to the middle of two neighboring lattice sites is identified as an SIA. Figure 3 illustrates the dynamics of $\langle 1\,1\,1 \rangle$ SIA diffusion in tungsten at 300 K. The atom S in figure 3(*a*) is an initial $\langle 1\,1\,1 \rangle$ SIA, which displaces its neighboring atoms (A, B, C and D) from their lattice sites. As the diffusion proceeds, one of the neighboring atoms (B or C) is displaced closest
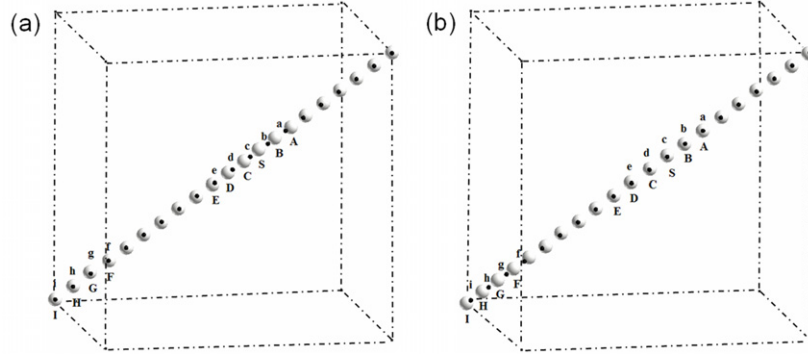
Figure 3. Typical diffusion process of SIA in tungsten at 300 K. The atoms labeled A–I are the tungsten atoms in the ⟨1 1 1⟩ string and are represented by the gray spheres. The corresponding lattice sites are labeled a–i and are represented by the black spheres. The atom S is the initial SIA. (*a*) $t = 0$ ps; (*b*) $t = 20$ ps.

to the middle of two neighboring lattice sites and acts as a new SIA. This process is repeated, leading to the migration of an SIA. As shown in figure 3(*b*), the atom G becomes a new SIA after 20 ps of system evolution. The atom S that is initially identified as an SIA occupies a lattice site (site b) that originally belonged to atom B. Except for the neighboring atoms of G that are displaced from their lattice sites, the atoms between atom S and G replace in turn their nearest neighboring atoms in the ⟨1 1 1⟩ direction toward the position of atom G. Thus, we conclude that the initial SIA initiates a sequence of tungsten atom displacements and replacements in ⟨1 1 1⟩ direction, and a new ⟨1 1 1⟩ SIA appears, accompanied by the annihilation of the old SIA.

For temperatures higher than 550 K, the migration proceeds in a three-dimensional manner due to the rotation of the ⟨1 1 1⟩ SIA configuration between three alternative crystallographically equivalent directions; for example, [1 1 1], [$\bar{1}$ $\bar{1}$ 1] or [$\bar{1}$ 1 1]. For example, figure 4 displays in detail this process at 550 K. The [1 1 1] SIA configuration, which migrates one-dimensionally in the [1 1 1] direction for most of the time, starts to rotate in the (1 1 0) surface when the system evolves for approximately 187 ps. After a system evolution of 1 ps, it transforms to the [1 1 0] SIA configuration, which is an intermediate configuration for the event of rotation of the SIA configuration between the [1 1 1] and [1 1 $\bar{1}$] directions. With further system evolution of approximately 1 ps, the [1 1 $\bar{1}$] SIA configuration forms. It will continue to migrate one-dimensionally in the [1 1 $\bar{1}$] direction until the next rotation occurs. Similar phenomena have been observed in the results of MD simulations using the DND and AT potentials [5, 18].

The diffusivity of SIAs in tungsten was studied by using the MD method on the basis of the Einstein relation, which is given by:

$$D = \lim_{t \to \infty} \frac{\langle R(t)^2 \rangle}{2\, d\, t}, \tag{7}$$

where $\langle R(t)^2 \rangle$ is the ensemble-averaged mean-square displacement of the SIA, t is the diffusion time, and d is the dimensionality of the space in which diffusion is occurring. The temperature of the system was varied between 100 and 500 K. Depending on the temperature of the system, the simulation time was in the range of 2 to 7 ns. Because of efficiency considerations, the cubic simulation box was kept as small as possible, with a side length of approximately 3.16 nm, containing 2000 tungsten atoms and one SIA. Note that, during the course of the simulation,
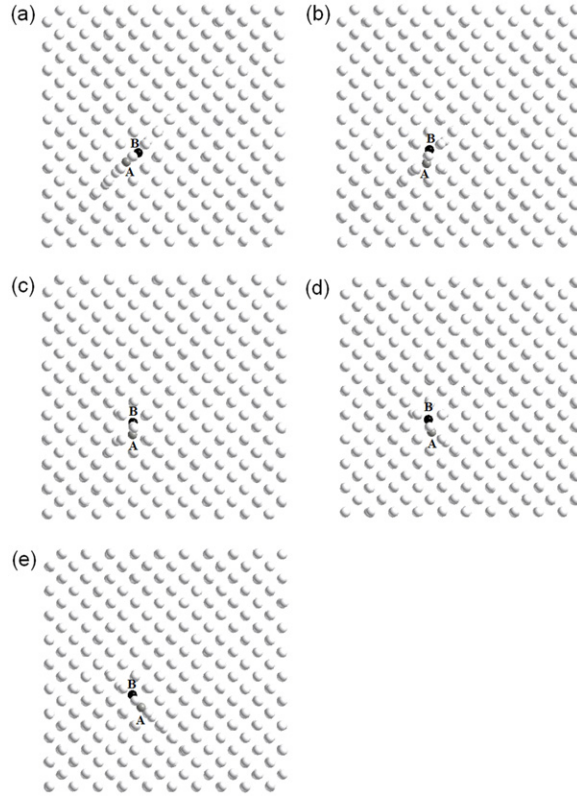
Figure 4. View of the SIA configuration consisting of the atoms A (gray sphere) and B (black sphere) in the [0 1 0] direction. (*a*) $t = 187$ ps; (*b*) $t = 187.8$ ps; (*c*) $t = 188$ ps; (*d*) $t = 188.2$ ps; (*e*) $t = 189$ ps.

as the SIA leaves the simulation box, one of its images will enter through the opposite face due to the periodic boundary conditions imposed. Consequently, the SIA always moves in the small simulation box, thus causing loss of information about the SIA diffusion However, as described in our previous work, the actual trajectory of the SIA in an infinite system can be achieved by correcting its position when an SIA migrates out of the simulation box [21].

Figure 5 displays the SIA diffusion coefficient over the temperature range of 100–500 K. The diffusion data was fitted by an Arrhenius law equation $D = D_0 \exp(-E_A/k_B T)$, with $D_0 = 1.82 \times 10^{-7}$ m^2 s^{-1} and $E_A = 0.022$ eV. In agreement with the other studies, this low migration energy indicates that SIAs in tungsten are very mobile. Recent MD simulations by Derlet *et al* using the DND potential indicate that the migration energy of an SIA in tungsten is 0.013 eV [18]. The experiments by Amano and Seidman [37] employing the filed-ion microscope technique demonstrated that SIAs underwent long-range migration and were mobile at temperatures as low as 28 K. The migration energy was found to be 0.079–0.085 eV. Dausinger and Schultz [38] concluded from their resistivity annealing experiments that SIA diffusion occurs between 24 and 30 K, corresponding to a migration energy of 0.054 eV. More recently, Tamimoto *et al* [39] proposed that SIA diffusion could already occur at temperatures below 1.5 K. Such a low migration temperature would correspond to a much lower migration energy than 0.054 eV. Thus, the migration energy of 0.022 eV determined in this work is reasonable.
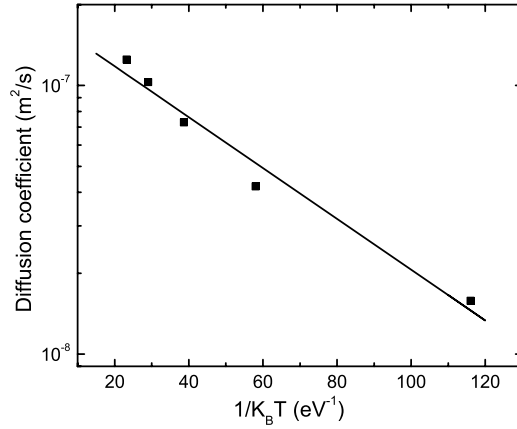
Figure 5. Diffusion coefficient for an SIA in tungsten, which is determined using MD simulations and plotted as a function of the absolute temperature T. The solid line is the Arrhenius relation fitted to the corresponding data over the temperature range from 100 to 500 K, with migration energy of 0.022 eV and a prefactor of $1.82 \times 10^{-7}\,\mathrm{m^2\,s^{-1}}$.

6. Extended defects

6.1. Surfaces

The correct prediction of surface properties is quite important for studying surface phenomena, such as surface modification, erosion and sputtering. Therefore, we have used the constructed potential to investigate the properties of three low-index surfaces: (1 0 0),(1 1 0) and (2 1 1).

The surface energies that are defined as the excess energy per surface unit area and interlayer relaxations for these three relaxed unreconstructed surfaces are presented in table 4. The surface energies determined from the FS potential presented here are lower than that calculated from the first-principles. However, it predicts the correct order of relative stability of these surfaces. The (1 1 0) surface is most stable due to its lowest surface energy. The (2 1 1) surface energy is slightly lower than the (1 0 0) surface energy, indicating that the (2 1 1) surface is more stable than (1 0 0) surface. In contrast, surface energies obtained from the AT potential are incorrectly ordered because the (2 1 1) surface energy is slightly higher than the (1 0 0) surface energy. Table 4 also shows the first and second interlayer spacings in all relaxed surfaces. Both the potential presented here and the AT potential predict the spacing of $\Delta_{12}^{1\,0\,0}$ with larger deviation in comparison with the experiment. However, the spacing of $\Delta_{12}^{2\,1\,1}$ obtained from the potential presented here agrees more closely with the experimental data.

6.2. Dislocations

It has been firmly established by many experimental and theoretical studies that the plastic properties of bcc metals are intimately linked with the core structures and mobility of $1/2\langle 1\,1\,1\rangle$ screw dislocations [47–50]. Here we focus on the core structures of $1/2\langle 1\,1\,1\rangle$ screw dislocations in bcc tungsten with the present potential by performing atomistic simulations, as in the previous studies [16, 51–54]. To obtain the core structure, we start by creating a perfect bcc crystal structure contained inside a cylindrical slab (diameter 50 lattice constants) with coordinate axes as follows: x parallel to $[1\,1\,\bar{2}]$, y parallel to $[1\,\bar{1}\,0]$, and z parallel to $[1\,1\,1]$. The dislocation with its Burgers vector along the z direction was inserted by displacing all

Table 4. Surface energies and interlayer relaxations for unreconstructed relaxed low-index surfaces obtained from experiment, DFT calculations, the AT potential, and the modified FS potential derived in the this study. γ^{hkl}: surface energy (mJ m^{-2}) for (hkl) surface; and Δ_{ij}^{hkl}: interlayer relaxation (%) between layer i and j.

	Experiment	DFT	AT[a]	This study
(100)				
γ^{100}		4636[b]	2924	2983
Δ_{12}^{100}	-6[c], -4 ± 10[d]	-6 ± 0.5[e]	-0.7	-0.9
Δ_{23}^{100}		0.5 ± 0.5[e]	-0.6	-0.7
(110)				
γ^{110}		4005[b]	2575	2549
Δ_{12}^{110}	-2.7 ± 0.5[f]	-3.6[g]	-0.5	-1.1
Δ_{23}^{110}	0.0 ± 0.3[f]	$+0.2$[g]	$+0.1$	$+0.02$
(211)				
γ^{211}		4177[b]	3046	2969
Δ_{12}^{211}	-9.3[h]		-4.8	-7.9
Δ_{23}^{211}			$+1.1$	$+5.0$

[a] Reference [16].
[b] Reference [40].
[c] Reference [41].
[d] Reference [42].
[e] Reference [43].
[f] Reference [44].
[g] Reference [45].
[h] Reference [46].

atoms in the slab according to the anisotropic elastic field of the dislocation [55]. The slab thickness is 5b, where b is the strength of Burgers vector. The simulation volume was divided into an inner region (containing 10830 atoms), in which the atoms were free to change their positions during the relaxation, and an outer region in which the atoms were fixed in their initial positions. Periodic boundary conditions were applied in the direction of the dislocation line ([111]) in order to simulate an infinite straight screw dislocation.

Figure 6 shows the relaxed core structure in tungsten using the usual differential displacement map [56]. The degenerate core was found with the potential presented here. However, the density-functional theory (DFT) predicts a non-degenerate core [57]. It is worth mentioning that the TB-BOP-potential, which is based on the tight-binding approximation, can also predict the correct core structure; however, the description of the short-range repulsion discourages the application of the TB-BOP to studies of point defects, in particular interstitials [16]. Up to now, there has been no potential of the FS or EAM type for bcc tungsten that would predict the non-degenerate core structure correctly. In fact, there is an ongoing discussion in the field about whether central-force potentials can predict the non-degenerate structure of $1/2\langle 111\rangle$ screw dislocations in bcc tungsten and other transition metals [16, 51, 58]. Recently, the work by Chiesa *et al* demonstrated that semi-empirical potentials based on the non-directional second moment approach FS approximation are able to reproduce the non-degenerate core structure if they correctly describe the inter-string pair potential of a rigid multi-string Frenkel–Kontorova model with the double hump structure of the energy versus string displacement curve [58]. Even so, constructing an FS or EAM potential for bcc tungsten with the correct point defect properties and screw dislocation structure is still a challenging task.
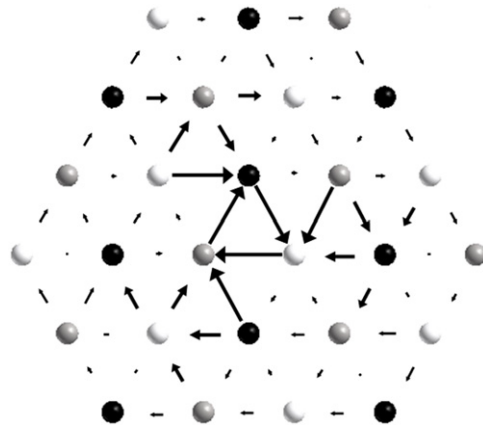
Figure 6. Core structure of the 1/2[1 1 1] screw dislocation relaxed using the potential presented here for tungsten using the differential displacement map. The atomic arrangement is shown in the projection perpendicular to the direction of the dislocation line, and circles represent atom positions in three successive (1 1 1) planes distinguished by shading. The arrows are drawn between pairs of neighboring atoms on the projections. The length of the arrows is proportional to the difference of the [1 1 1] displacements of the neighboring atoms, and normalized such that the longest arrow is equal to the separation of the atoms in the projection.

7. Conclusions

Due to the important influence of the W–W potential on the defect properties and the shortcomings of the currently available FS potential, in this paper, based on *ab initio* calculations, a modified FS-type interatomic potential for W–W interactions was developed. This potential is able to reproduce the correct SIA formation energies in tungsten, offering a significant improvement over the W–W potential by Ackland *et al*. Furthermore, the modified potential was applied to study in detail the diffusion of an SIA in tungsten. An Arrhenius fit to the diffusion data determined the migration energy to be 0.022 eV, which is in reasonable agreement with the experimental data. The observed migration of a $\langle 1\,1\,1\rangle$ SIA is one-dimensional in the $\langle 1\,1\,1\rangle$ direction at temperatures below 550 K. By investigating in detail the diffusion process, we have shown that the initial SIA initiates a sequence of tungsten atom displacements and replacements in the $\langle 1\,1\,1\rangle$ direction, and a new $\langle 1\,1\,1\rangle$ SIA appears that is accompanied by the annihilation of the old SIA. For temperatures higher than 550 K, the SIA migration begins to be three-dimensional in character as a result of the rotation of the $\langle 1\,1\,1\rangle$ SIA between three alternative crystallographically equivalent directions. Similar phenomena have been observed in the results of MD simulations using either the DND potential or the AT potential. The modified potential developed in this paper can be used to investigate SIA properties and diffusion. We have used the constructed potential to investigate the surface properties and core structures of $1/2\langle 1\,1\,1\rangle$ screw dislocations, which predicts the correct order of relative stability for three low-index surfaces: (1 0 0), (1 1 0) and (2 1 1). The core structure is predicted to be degenerate, while the DFT predicts a non-degenerate core. Note that, similar to the AT and DND potentials, we do not include a short-range correction to this potential, which is necessary in studying high-energy collision dynamics. To simulate high-energy collision cascades, one can employ the approach presented by Fikar and Schaublin [5] to improve the reliability of the potential at short-range.

In addition, the thermal expansion, which is a fundamental physical property of materials, is calculated using this modified potential over a temperature range from 0 to 3500 K. The results are in reasonable agreement with the experimental data, thereby overcoming the shortcoming of the predicted negative thermal expansion using the W–W potential developed by Derlet *et al*. These results demonstrate that the potential presented here is valid over a fairly broad temperature range. We expect that the potential (which is constructed in such a way as to be able to retain a sufficiently high accuracy over a range of strongly distorted atomistic configurations and over a broad temperature range) will help us to understand defect behavior and its effect on the microstructural and mechanical properties of tungsten.

Acknowledgments

References

[1] Janeschitz G 2001 *J. Nucl. Mater.* **290–293** 1
[2] Bolt H, Barabash V, Krauss W, Linke J, Neu R, Suzuki S and Yoshida N 2004 *J. Nucl. Mater.* **329–333** 66
[3] Gumbsch P, Reiedle J, Hartmaier A and Fischmeister H F 1998 *Science* **282** 1293
[4] Fikar J and Schaublin R 2009 *Nucl. Instrum. Methods Phys. Res.* B **267** 3218
[5] Fikar J and Schaublin R 2009 *J. Nucl. Mater.* **386–388** 97
[6] Li M, Cui J C, Wang J and Hou Q 2013 *J. Nucl. Mater.* **433** 17
[7] Becquart C S and Domain C 2006 *Phys. Rev. Lett.* **97** 196402
[8] Becquart C S and Domain C 2007 *Nucl. Instrum. Methods Phys. Res.* B **255** 23
[9] Becquart C S and Domain C 2009 *J. Nucl. Mater.* **385** 223
[10] Nguyen-Manh D, Horsfield A P and Dudarev S L 2006 *Phys. Rev.* B **73** 020101
[11] Finnish M W and Sinclair J E 1984 *Phil. Mag.* A **50** 45
[12] Daw M S and Baskes M I 1984 *Phys. Rev.* B **29** 6443
[13] Lee B J, Baskes M I, Kim H and Cho Y K 2001 *Phys. Rev.* B **64** 184102
[14] Juslin N, Erhart P, Traskelin P, Nord J, Herriksson K O E, Nordlund K, Salonen E and Albe K 2005 *J. Appl. Phys.* **98** 123520
[15] Ahlgren T, Heinola K, Juslin N and Kuronen A 2010 *J. Appl. Phys.* **107** 033516
[16] Mrovec M, Gröger R, Bailey A G, Nguyen-Manh D, Elsässer C and Vitek V 2007 *Phys. Rev.* B **75** 104119
[17] Ackland G J and Thetford R 1987 *Phil. Mag.* A **56** 15
[18] Derlet P M, Nguyen-Manh D and Dudarev S L 2007 *Phys. Rev.* B **76** 054107
[19] White G K and Minges M L 1997 *Int. J. Thermophys.* **18** 1269
[20] Wang K and Reeber R R 1998 *Mater. Sci. Eng.* R **23** 101
[21] Wang J, Zhou Y L, Li M and Hou Q 2012 *J. Nucl. Mater.* **427** 290
[22] Winte G 1995 *Genetic Algorithm in Engineering and Computer Science* (New York: Wiley)
[23] Juslin N and Wirth B D 2013 *J. Nucl. Mater.* **432** 61
[24] Li X C, Shu X L, Liu Y N, Gao F and Lu G H 2011 *J. Nucl. Mater.* **408** 12
[25] Dai X D, Kong Y, Li J H and Liu B X 2006 *J. Phys.: Condens. Matter* **18** 4527
[26] Satta A, Willaime F and de Gironcoli S 1998 *Phys. Rev.* B **57** 11184
[27] Ochs T, Beck O, Elsasser C and Meyer B 2000 *Phil. Mag.* A **80** 351
[28] Kittel C 1996 *Introduction to Solid State Physics* 7th edn (New York: Wiley)
[29] Lide D R 2004 *Handbook of Chemistry and Physics* 85th edn (Boca Raton, FL: CRC Press)

[30] Einarsdotter K, Sadigh B, Grimvall G and Ozolins V 1997 *Phys. Rev. Lett.* **79** 2073
[31] Bolef D I and de Klerk J 1962 *J. Appl. Phys.* **33** 2311
[32] Wollenberger H J 1983 *Physical Metallurgy* (Amsterdam: North-Holland)
[33] Maier K, Peo M, Saile B, Schaefer H E and Seeger A 1979 *Phil. Mag.* A **40** 701
[34] Balluffi R W 1978 *J. Nucl. Mater.* **69–70** 240
[35] Mundy J N, Ockers S T and Smedskjaer L C 1987 *Phil. Mag.* A **56** 851
[36] Lassner E and Schubert W D 1999 *Tungsten Properties, Chemistry, Technology of the Element, Alloy, and Chemical Compounds* (New York: Kluwer Academic/ Plenum)
[37] Amano J and Seidman D N 1984 *J. Appl. Phys.* **56** 983
[38] Dausingere F and Schultz H 1975 *Phys. Rev. Lett.* **35** 1773
[39] Tamimoto H, Mizubayashi H and Okuda S 1996 *J. Phys.* IV **6** 285
[40] Vitos L, Ruban A V, Skriver H L and Kollar J 1998 *Surf. Sci.* **411** 186
[41] Fu C L and Freeman A J 1988 *Phys. Rev.* B **37** 2685
[42] Altman M S, Estrup P J and Robinson I K 1988 *Phys. Rev.* B **38** 5211
[43] Yu R, Krakauer H and Singh D 1992 *Phys. Rev.* B **45** 8671
[44] Meyerheim H L, Sander D, Popescu R, Steadman P, Ferrer S and Kirschner J 2001 *Surf. Sci.* **475** 103
[45] Arnold M, Hupfauer G, Bayer P, Hammer L, Heinz K, Kohler B and Scheffler M 1997 *Surf. Sci.* **382** 288
[46] Grizzi O, Shi M, Bu H, Rabalais J W and Hochmann P 1989 *Phys. Rev.* B **40** 10127
[47] Christian J W 1983 *Metall. Trans.* A **14** 1237
[48] Vitek V 2005 *Encyclopedia of Solid State Physics* (Oxford: Elsevier)
[49] Duesbery M S 1989 *Dislocations in Solids* (Amsterdam: North-Holland)
[50] Taylor G 1992 *Prog. Mater. Sci.* **36** 29
[51] Mrovec M, Nguyen-Manh D, Pettifor D G and Vitek V 2004 *Phys. Rev.* B **69** 094115
[52] Duesbery M S and Vitek V 1998 *Acta Mater.* **46** 1481
[53] Gröger R, Bailey A G and Vitek V 2008 *Acta Mater.* **56** 5401
[54] Gröger R and Vitek V 2009 *Phil. Mag.* **89** 3163
[55] Hirth J P and Lothe J 1982 *Theory of Dislocations* (New York: Wiley-Interscience)
[56] Vitek V 1974 *Cryst. Latt. Defects* **5** 1
[57] Frederiksen S L and Jacobsen K W 2003 *Phil. Mag.* **83** 365
[58] Chiesa S, Gilbert M R, Dudarev S L, Derlet P M and Van Swygenhoven H 2009 *Phil. Mag.* **89** 3235